A Single Mutation in the Nonamyloidogenic Region of Islet Amyloid Polypeptide Greatly Reduces Toxicity[†]

Jeffrey R. Brender,[‡,§] Kevin Hartman,[‡,§] Kendra R. Reid,[‡] Robert T. Kennedy,[‡] and Ayyalusamy Ramamoorthy*[,‡,§]

Departments of Chemistry and Biophysics, University of Michigan, Ann Arbor, Michigan 48109-1055

Received July 30, 2008; Revised Manuscript Received September 24, 2008

ABSTRACT: Islet amyloid polypeptide (IAPP or amylin) is a 37-residue peptide secreted with insulin by β-cells in the islets of Langerhans. The aggregation of the peptide into either amyloid fibers or small soluble oligomers has been implicated in the death of β-cells during type 2 diabetes through disruption of the cellular membrane. The actual form of the peptide responsible for β-cell death has been a subject of controversy. Previous research has indicated that the N-terminal region of the peptide (residues 1−19) is primarily responsible for the membrane-disrupting effect of the hIAPP peptide and induces membrane disruption to a similar extent as the full-length peptide without forming amyloid fibers when bound to the membrane. The rat version of the peptide, which is both noncytotoxic and nonamyloidogenic, differs from the human peptide by only one amino acid residue: Arg18 in the rat version while His18 in the human version. To elucidate the effect of this difference, we have measured in this study the effects of the rat and human versions of $IAPP_{1-19}$ on islet cells and model membranes. Fluorescence microscopy shows a rapid increase in intracellular calcium levels of islet cells after the addition of $hIAPP_{1-19}$, indicating disruption of the cellular membrane, while the rat version of the $IAPP_{1-19}$ peptide is significantly less effective. Circular dichroism experiments and dye leakage assays on model liposomes show that $rIAPP_{1-19}$ is deficient in binding to and disrupting lipid membranes at low but not at high peptide to lipid ratios, indicating that the ability of $rIAPP_{1-19}$ to form small aggregates necessary for membrane binding and disruption is significantly less than $hIAPP_{1-19}$. At pH 6.0, where H18 is likely to be protonated, $hIAPP_{1-19}$ resembles $rIAPP_{1-19}$ in its ability to cause membrane disruption. Differential scanning calorimetry suggests a different mode of binding to the membrane for $rIAPP_{1-19}$ compared to $hIAPP_{1-19}$. Human $IAPP_{1-19}$ has a minimal effect on the phase transition of lipid vesicles, suggesting a membrane orientation of the peptide in which the mobility of the acyl chains of the membrane is relatively unaffected. Rat $IAPP_{1-19}$, however, has a strong effect on the phase transition of lipid vesicles at low concentrations, suggesting that the peptide does not easily insert into the membrane after binding to the surface. Our results indicate that the modulation of the peptide orientation in the membrane by His18 plays a key role in the toxicity of nonamyloidogenic forms of hIAPP.

It has been known for many years that insoluble, highly aggregated amyloid deposits of human islet amyloid polypeptide protein (hIAPP,[1] also known as amylin) are found postmortem in the islets of Langerhans of pancreatic β-cells in the majority (>90%) of type 2 diabetic patients but not in nondiabetic patients of the same age cohort (*1*). The high tissue visibility of the amyloid deposits and their prevalence in diabetic patients have led to the hypothesis that the formation of amyloid fibers plays a causative role in the development of the disease (*2, 3*).

Human: KCNTATCATQRLANFLVHSSNNFGAILSSTNVGSNTY

Mouse/Rat: KCNTATCATQRLANFLVRSSNNLGPVLPPTNVGSNTY

FIGURE 1: Amino acid sequences of rat and human IAPP. The 1−19 fragment that is used in this study is shown in blue, and the differences between the two sequences are shown in red. A disulfide bond exists between residues 2 and 8. The C-termini are amidated like the naturally occurring peptide.

The hypothesis that extracellular amyloid fibers directly cause β-cell apoptosis has been challenged by both *in vitro* and *in vivo* studies. Transgenic mice models have been particularly useful in this respect as rats do not spontaneously develop type 2 diabetes and have an IAPP variant that is both noncytotoxic and nonamyloidogenic (Figure 1) (*4*). Transgenic mice expressing the human version of IAPP develop complications with metabolic characteristics similar to human type 2 diabetes (*5*−*8*). However, there is poor spatial and temporal overlap between amyloid formation and β-cell apoptosis in transgenic mice. Extracellular amyloid in homozygous transgenic mice is only detected after the

[†] This study was supported by research funds from the Michigan Diabetes Research Training Center at the University of Michigan and the NIH (AI054515 to A.R. and DK046960 to R.T.K.).

* Corresponding author: e-mail, ramamoor@umich.edu; phone, (734) 647-6572; fax, (734) 763-2307.

[‡] Department of Chemistry, University of Michigan.

[§] Department of Biophysics, University of Michigan.

[1] Abbreviations: CD, circular dichrosim; DMPC, 1,2-dimyristoyl-*sn*-glycero-3-phosphocholine; DMPG, 1,2-dimyristoyl-*sn*-glycero-3-phospho-*rac*-(1-glycerol); DMSO, dimethyl sulfoxide; DSC, differential scanning calorimetry; HFIP, 1,1,1,3,3,3-hexafluoro-2-propanol; hIAPP, human islet amyloid polypeptide; IAPP, islet amyloid polypeptide; NMR, nuclear magnetic resonance; POPG, 1-palmitoyl-2-oleoyl-*sn*-glycero-3-phospho-*rac*-(1-glycerol); rIAPP, rat islet amyloid polypeptide.

10.1021/bi801427c CCC: $40.75
Published on Web 11/07/2008

phase of rapid β-cell death has passed, and the β-cells undergoing apoptosis are not adjacent to amyloid fibers (*9*−*11*). Furthermore, some transgenic mice models expressing hIAPP form extensive amyloid fiber deposits but do not develop type 2 diabetes (*12*). The lack of correlation between islet amyloid formation and the pathology of type 2 diabetes in transgenic mice mirrors findings in humans, in that islet amyloid is found in people without diabetes as well as not found in all people with diabetes (*13, 14*). Studies directly measuring the effect of IAPP upon β-cells have confirmed the relatively low toxicity of mature amyloid fibers of IAPP (*15*−*19*).

Unlike mature fibers, small hIAPP oligomers have been demonstrated to be cytotoxic to β-cells (*5, 15*−*18, 20, 21*). Soluble oligomers of IAPP, in common with other amyloidogenic proteins, have been implicated in the disruption of cellular homeostasis either by the formation of relatively nonselective ion channels or by direct fragmentation of the cellular membrane (*22, 23*). The kinetics of oligomer formation is complex and is likely to involve multiple pathways (*24*−*26*). Inhibition studies have suggested that the toxic oligomers are a distinct species of amyloid proteins and not simply direct intermediates of mature fibers. Inhibitors have been found that suppress the formation of toxic oligomers but not the formation of amyloid fibers (*27*). Conversely, other inhibitors have been shown to have the opposite effect, suppressing the formation of amyloid fibers but not the formation of toxic oligomers (*18, 27*). The ability of some inhibitors to suppress the formation of small oligomers independently of their effect on the formation of amyloid fibers suggests the toxic oligomers are at least partly off the kinetic pathway for the formation of amyloid fibers.

Although amyloidogenic proteins can disrupt membranes through the formation of toxic oligomers, new evidence suggests the formation of toxic oligomers may not be unique to amyloidogenic proteins. An antibody specific for the soluble oligomeric form of amyloidogenic proteins also recognizes several nonamyloidogenic pore-forming proteins (*28*). More directly, the N-terminal fragment of human IAPP (residues 1−19) has been found to disrupt synthetic vesicles to nearly the same extent as full-length IAPP but does not form amyloid fibers while bound to the membrane (*25*). Significantly, the sequences of human IAPP and rat IAPP are identical in this region of the protein except for residue 18, which is His in the human version and Arg in the rat version of the peptide (Figure 1). In a companion paper of this issue, high-resolution structures of $hIAPP_{1-19}$ and $rIAPP_{1-19}$ in DPC micelles were solved by solution NMR. Although the structures are largely similar, $rIAPP_{1-19}$ is more disordered at the N-terminus than the $hIAPP_{1-19}$ peptide. More significantly, $hIAPP_{1-19}$ is shielded from the paramagnetic quencher Mn^{2+} while $rIAPP_{1-19}$ is exposed. The difference in the accessibility of Mn^{2+} to the two peptides when bound to DPC micelles suggests $rIAPP_{1-19}$ adopts a different orientation in the membrane than $hIAPP_{1-19}$. This effect is likely due to the difference in charge at residue 18, as $hIAPP_{1-19}$ becomes significantly more solvent exposed at pH 6.0 where the histidine residue is likely to be ionized. To see the impact of this difference on the toxicity of the two peptides, we have performed *in vivo* and *in vitro* assays of the ability of the two peptides to permeabilize the membranes of both β-cell islets and model membranes. We report here that the $rIAPP_{1-19}$ peptide is significantly impaired in its ability to disrupt phospholipid membranes compared to the corresponding $hIAPP_{1-19}$ peptide, highlighting the role of this key residue in controlling the toxicity of the peptide.

MATERIALS AND METHODS

Materials. POPG (1-palmitoyl-2-oleoyl-*sn*-glycero-3-phospho-*rac*-(1-glycerol)), DMPG (1,2-dimyristoyl-*sn*-glycero-3-phospho-*rac*-(1-glycerol)), and DMPC (1,2-dimyristoyl-*sn*-glycero-3-phosphocholine) phospholipids were obtained from Avanti (Alabaster, AL); DMSO (dimethyl sulfoxide), carboxyfluorescein, and HFIP (1,1,1,3,3,3-hexafluoro-2-propanol) were obtained from Sigma-Aldrich; $hIAPP_{1-19}$ and $rIAPP_{1-19}$ with amidated C-termini (>95% purity) were purchased from Genscript. Before use, lyophilized $rIAPP_{1-19}$ and $hIAPP_{1-19}$ were dissolved in HFIP at a concentration of 10 mg/mL for 1 h to break up any preformed aggregates present in the solution. Aliquots of the peptide stock solution were flash-frozen in liquid nitrogen and then lyophilized again for more than 16 h at less than 1 mTorr vacuum to completely remove HFIP. All experiments were conducted at room temperature (approximately 23 °C). POPG vesicles for the circular dichroism and dye leakage experiments were prepared as previously described (*25*).

Islet Isolation Protocol. Pancreatic islets were obtained from 20 to 30 g male CD-1 mice as previously described (*29*). Briefly, mice were sacrificed by cervical dislocation, and collagenase type XI was injected into the pancreas through the main pancreatic duct. The pancreas was removed and incubated in 5 mL of a collagenase solution at 37 °C. Islets that were used for experiments were 100−200 μm in diameter, had an intact islet membrane, and were oblong to spherical in shape. Islets were placed in tissue culture dishes and incubated in RPMI 1640 containing 10% fetal bovine serum, 100 units/mL penicillin, and 100 μg/mL streptomycin at 37 °C, 5% CO_2, pH 7.4. Islets were used 1−6 days following isolation.

Intracellular Ca^{2+} Measurements. Calcium flux measurements were performed on islets after a 40 min incubation with 2 μM fluorescent calcium-sensitive dye, fura-2. Afterward, individual islets were loaded into an open cell chamber on a microfluidic chip. Islet media and stimulants were perfused over the islet at a rate of 0.6 μL/min. The chip was placed atop the stage of a Nikon Diaphot 300 microscope. The fura-2 was alternately excited using a filter wheel with 340 and 380 nm light from a xenon arc lamp. The fluorescence emission from both excitation wavelengths was collected through a 510 ± 10 nm bandpass filter. Images of the islet were collected at 1 Hz, and the intensity over islet area was integrated using Metamorph software. Intracellular calcium concentration was calculated by determining the ratio of the emission at 340 and 380 nm excitation after calibration of the system.

Circular Dichroism Spectroscopy. Lyophilized peptide was dissolved in sodium phosphate buffer (10 mM, pH 7.3), briefly vortexed and sonicated (approximately 15 s), and transferred to a 0.1 cm cuvette. After the initial spectrum of the peptide in solution was taken, POPG vesicles from a 40 mg/mL stock solution were titrated into the cuvette. Spectra were measured at 1 nm intervals from 185 to 260 nm at a

scanning speed of 50 nm/min and a bandwidth of 5 nm. Each spectrum reported is the average of four scans after subtraction of the baseline spectrum of buffer and vesicles without peptide.

Dye Leakage Assay. For the dye leakage experiments, carboxyfluorescein containing POPG vesicles was prepared by rehydrating the dried lipid film in 50 mM sodium phosphate buffer (pH 7.5) containing 40 mM carboxyfluorescein, adjusted to pH 7.5 by the addition of sodium hydroxide. Nonencapsulated carboxyfluorescein was removed from the vesicles through size exclusion chromatography using a PD-10 column (Amersham Pharmacia Biotech, Uppsala, Sweden). Vesicle solutions were used immediately, and a fresh vesicle solution was used for each experiment. Fluorescence readings were taken at an excitation wavelength of 493 nm and an emission wavelength of 518 nm. A baseline reading was taken on the solutions prior to the addition of the peptide. After injection, the fluorescence intensity was recorded after 100 s of interaction. The fluorescence signal given by the addition of peptide was then normalized by the addition of Triton X detergent, causing all vesicles present to release any remaining dye to obtain the total possible fluorescent signal.

Differential Scanning Calorimetry. Multilamellar vesicles of DMPC and DMPG (70% DMPC, 30% DMPG) were prepared as described for the dye leakage experiments. Sodium phosphate buffer (10 mM) with 150 mM NaCl at pH 7.3 was used to hydrate the samples. The total molar concentration of lipid was kept constant (5.9 mM) for each sample while the molar peptide concentration was varied as indicated. Scans were run on a Calorimetry Sciences N-DSC II over a temperature range of 5−45 °C with a total of four heating and four cooling scans. The heating scans were run at 0.25 °C/min while the cooling scans were run at 1.0 °C/min, in between each of which there was a 10 min equilibration period. The buffer solution without the sample was used as the reference cell. The data were converted to molar heat capacity using the average molecular weight of the lipids, the lipid concentration, and a partial specific volume of 0.988 mL/g. Excess heat capacity was calculated by subtracting a baseline with buffer in both the reference and sample cells at the same scanning rate.

RESULTS AND DISCUSSION

Membrane Disruption Induced by hIAPP$_{1-19}$ and rIAPP$_{1-19}$ in POPG Vesicles. To test for differences in the extent of membrane disruption induced by hIAPP$_{1-19}$ and rIAPP$_{1-19}$ peptides, leakage of the dye carboxyfluorescein from large unilamellar POPG vesicles (Figure 2) was measured as a function of the concentration of POPG at three different concentrations of the peptide. Carboxyfluorescein in intact vesicles is at a high concentration (40 mM) and self-quenched. Disruption of the membrane of the vesicle by the peptide allows carboxyfluorescein to escape, eliminating the self-quenching effect and therefore increasing fluorescence of carboxyfluorescein. For each graph in Figure 2, the peptide-to-lipid-ratio was varied by the addition of empty POPG vesicles (that is, vesicles not containing carboxyfluorescein) while the concentrations of peptide and carboxyfluorescein-containing vesicles were kept constant. Decreasing the peptide-to-lipid ratio in this manner has two

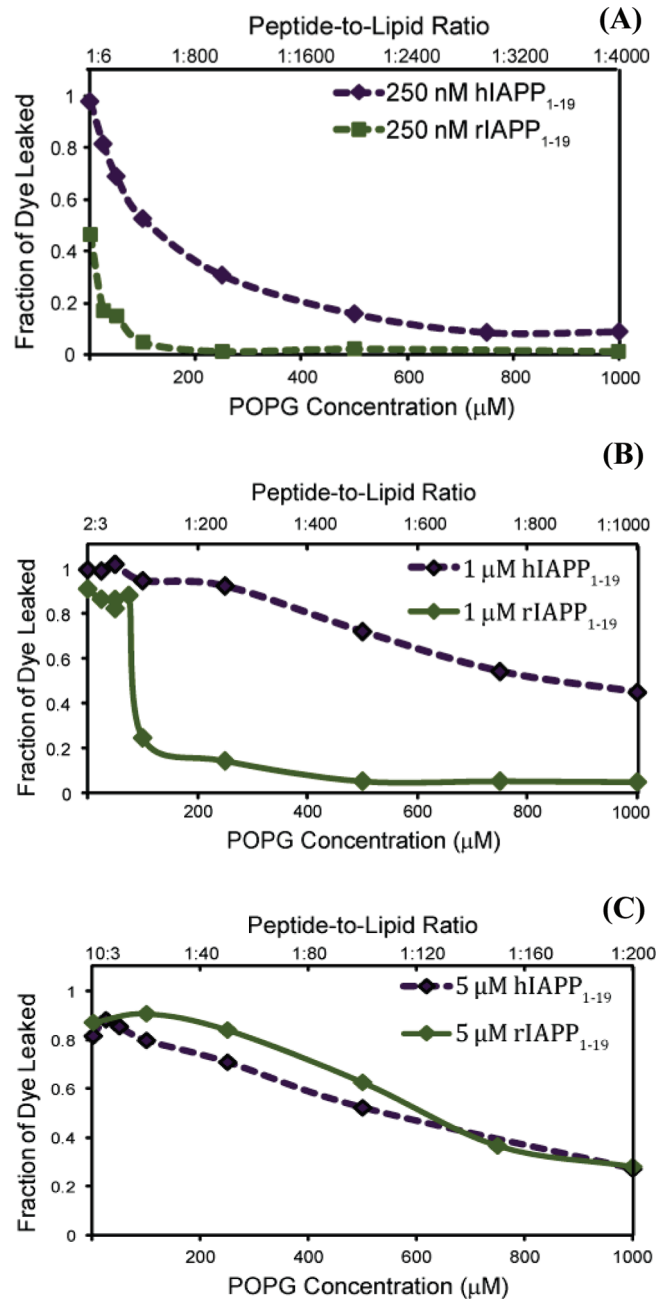

FIGURE 2: Liposome leakage induced by hIAPP$_{1-19}$ (blue diamonds) and the rIAPP$_{1-19}$ fragment (green diamonds) at pH 7.5. The peptide-to-lipid ratio was varied by adding 250 nM (A), 1 μM (B), and 5 μM (C) solutions of either rIAPP$_{1-19}$ or hIAPP$_{1-19}$ to POPG liposomes containing carboxyfluorescein (1.5 μM) and enough empty POPG liposomes (not containing carboxyfluorescein) to create the indicated molar ratio of peptide to lipid. The fluorescence signal was recorded at 100 s after peptide injection and normalized to the total possible signal upon addition of detergent.

effects. First, peptide binding and membrane disruption for empty vesicles not containing carboxyfluorescein are not detected. Binding of peptide to empty vesicles reduces the amount of peptide available to bind to carboxyfluorescein-containing vesicles. The membrane disruption induced by the peptide should accordingly decrease in a near-linear fashion as the amount of empty vesicles is increased (values to the right on the *x*-axis in Figure 2). Second, the amount of peptide bound to each vesicle is decreased as the total lipid concentration is increased. If the process of membrane disruption is nonlinearly dependent on the concentration of

the peptide bound to the membrane, the amount of membrane disruption can also be expected to be nonlinearly dependent on the peptide-to-lipid ratio. This can occur if either the peptide oligomerizes to form peptide channels in the membrane or if membrane disruption occurs by a weakening of the membrane via a carpet-type mechanism as reported for antimicrobial peptides (*30*−*32*).

Human $IAPP_{1-19}$ strongly induced membrane disruption at all concentrations tested (Figure 2). Membrane disruption decreased as the peptide-to-lipid ratio is decreased, but the plots are relatively linear for peptide concentrations of 1 and 5 μM (Figure 2B,C). Only at the lowest peptide concentration of 250 nM is a nonlinear dependence of membrane disruption on the concentration of POPG apparent. At a 5 μM peptide concentration, $rIAPP_{1-19}$ is slightly more effective than $hIAPP_{1-19}$ at disrupting the membrane (Figure 2C). This effect is most likely due to the greater charge on the $rIAPP_{1-19}$ peptide at pH 7.3 (+4 vs +3 for the $hIAPP_{1-19}$ assuming H18 is uncharged at pH 7.5) which facilitates partitioning into membranes containing anionic lipids. At a lower peptide concentration (1 μM, Figure 2B), $rIAPP_{1-19}$ shows a striking nonlinear dependence on the peptide-to-lipid ratio. At high peptide-to-lipid molar ratios, the $rIAPP_{1-19}$ peptide is nearly as effective as the $hIAPP_{1-19}$ peptide. However, as the peptide-to-lipid ratio is decreased, the membrane-disrupting activity of $rIAPP_{1-19}$ is abruptly lost, dropping off suddenly as a critical peptide-to-lipid ratio is surpassed (approximately 1:100). At the lowest peptide concentration tested in this study, $rIAPP_{1-19}$ induces significant membrane disruption only at the highest peptide-to-lipid ratio (1:6) measured (Figure 2C).

The physiologically relevant peptide-to-lipid ratio is difficult to establish exactly, as IAPP is stored at high concentrations (0.8−4 mM) in secretory granules before being released into the bloodstream (*33*). After release from the secretory granule, the peptide is diluted in the bloodstream to quite low concentrations (*34*). While the equilibrium concentration of IAPP in the bloodstream is quite low, islet cells are briefly exposed to high concentrations of IAPP immediately upon the release of IAPP from the secretory granule. The amount of IAPP bound to the islet membrane and the consequent peptide-to-lipid ratio therefore depend on a variety of factors that are poorly understood at present, including the dynamics of the release of IAPP from the secretory granule, the reversibility of the membrane binding process, and the affinity for IAPP for the cellular membrane. It is also important to note that cell membranes, unlike model membranes, are highly heterogeneous, and it is probable that IAPP is concentrated in certain regions of the cell membrane, an effect seen previously for the related $A\beta_{1-40}$ peptide (*35, 36*). In light of the uncertainty about the kinetics of the process of IAPP release from the secretory granule and also the binding of IAPP to the β-cell membrane, it is difficult to establish a narrow range of peptide-to-lipid ratios as being physiologically relevant. Nevertheless, low peptide-to-lipid ratios are more likely to be physiologically relevant than high peptide-to-lipid ratios as the equilibrium concentration of IAPP is low.

Human IAPP differs from $rIAPP_{1-19}$ only by the H18R substitution. At the slightly alkaline pH of the extracellular matrix (~7.3), H18 will be deprotonated while R18 will remain charged. This ionization state of H18 has previously been shown to have an effect on the fibrillization of full-length hIAPP, with hIAPP fibrillizing faster at acidic pH where H18 is charged (*37, 38*). To test the effect of the ionization state of H18 on the membrane disruption, the vesicle disruption assay was repeated at pH 6.0 using 1 μM $hIAPP_{1-19}$ or $rIAPP_{1-19}$ (Figure 3). The ionization state at residue 18 appears to be critical for membrane disruption, as $hIAPP_{1-19}$ causes significantly less disruption at lower peptide-to-lipid ratios at pH 6.0 than at pH 7.3 (compare Figure 2B and Figure 3). The amount of disruption induced by $hIAPP_{1-19}$ at pH 6.0 is very similar to $rIAPP_{1-19}$, suggesting $hIAPP_{1-19}$ disrupts liposomes by a similar mechanism as $rIAPP_{1-19}$ at pH 6.0 but not at pH 7.3 where histidine is deprotonated.

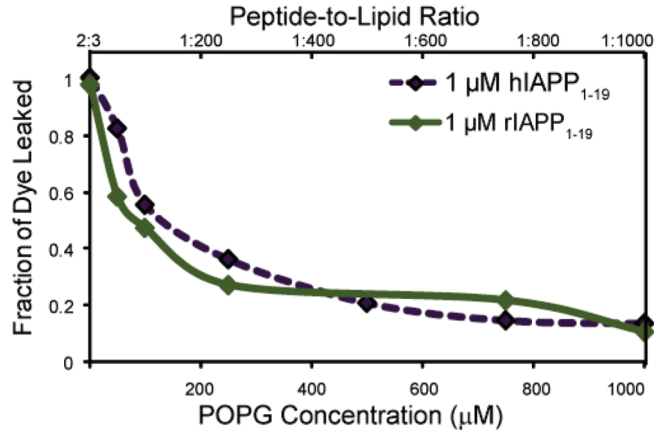

FIGURE 3: Liposome leakage induced by $hIAPP_{1-19}$ (blue diamonds) and the $rIAPP_{1-19}$ fragment (green diamonds) at pH 6.0. Except for the pH, the liposome leakage assay was performed as indicated for the pH 7.3 sample using 1 μM solutions of either $rIAPP_{1-19}$ or $hIAPP_{1-19}$.

The pH dependence of membrane disruption for $hIAPP_{1-19}$ is supported by the paramagnetic quenching experiments detailed in the companion paper (*39*). Human $IAPP_{1-19}$ in DPC micelles is strongly quenched by Mn^{2+} at pH 6.0 but not at pH 7.3. Rat $IAPP_{1-19}$, by contrast, is strongly quenched at pH 7.3. As the Mn^{2+} ion quenches the signals of residues near the membrane−solution interface, it is expected that a surface-associated peptide will be more strongly quenched than a peptide more deeply inserted into the membrane. The enhancement of paramagnetic quenching of $hIAPP_{1-19}$ at pH 6.0 indicates $hIAPP_{1-19}$ binds closer to the surface of the micelle when H18 is protonated, adopting a surface-associated binding mode similar to $rIAPP_{1-19}$.

Membrane Disruption Induced by $hIAPP_{1-19}$ and $rIAPP_{1-19}$ in Pancreatic Islets. The results of the dye leakage assay indicate $hIAPP_{1-19}$ strongly disrupts phospholipid membranes; on the other hand, $rIAPP_{1-19}$ also disrupts phospholipid membranes if the peptide-to-lipid ratio is high enough. These results are in agreement with our previous study which showed that the $hIAPP_{1-19}$ fragment, which is nonamyloidogenic if bound to a membrane, disrupted POPG vesicles to a similar extent as the strongly amyloidogenic full-length IAPP peptide (*25*). However, all of these assays were performed under conditions that maximized peptide binding (low ionic strength, high content of anionic lipids) and differ from the conditions found in the *in vivo* setting. A more accurate assessment of the damage induced by IAPP could be done by the use of cells loaded with a calcium

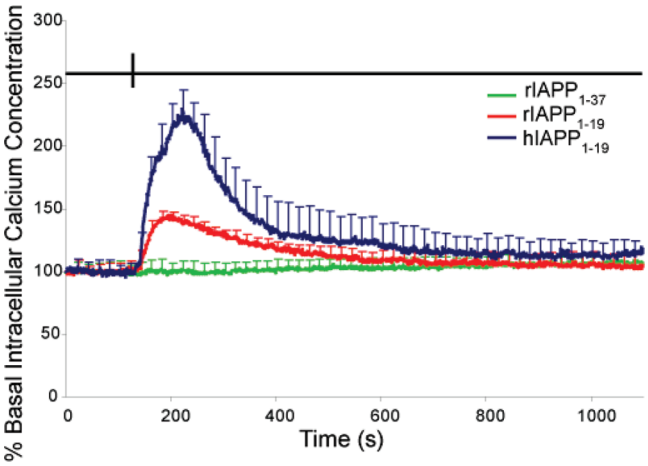

FIGURE 4: Membrane permeabilization in pancreatic islets induced by IAPP. Whole mouse pancreatic islets were loaded 45 min prior to the experiment with 2 μM calcium-sensitive dye fura-2 AM. At 140 s (indicated by a vertical line at the top) 12 μg/mL $hIAPP_{1-19}$, $rIAPP_{1-19}$, or $rIAPP_{1-37}$ was perfused over the cells. The values given are the average of five islet samples; error bars indicate standard error of the mean.

sensitive dye to monitor changes in intracellular calcium levels due to the membrane permeabilization induced by IAPP (*15, 40*−*43*). Full-length hIAPP is known to disrupt the calcium homeostasis of neuroblastoma (SH-SY5Y) cells in a conformation-dependent manner (*15*). Demuro et al. have shown that the addition of monomeric hIAPP and mature fibers of hIAPP had little effect on intercellular calcium levels but the addition of a prefibrillar oligomeric form of hIAPP caused the influx of calcium into the cell. The rise in intercellular calcium concentrations induced by prefibrillar oligomeric hIAPP was dependent on the concentration of hIAPP used, with a maximal response at 12 μg/mL and an EC_{50} of approximately 3.5 μg/mL (*15*). The membrane disruption induced by hIAPP was large enough to permit leakage of calcein dye from the cell, indicating that prefibrillar oligomeric hIAPP does not simply disrupt calcium homeostasis by the activation of endogenous calcium channels (*15*) as has been reported for the fibrillar form of hIAPP (*43*).

To test the toxic effect of $hIAPP_{1-19}$ and $rIAPP_{1-19}$ peptides on pancreatic islets, we performed an analogous experiment by measuring the influx of calcium into single islets upon the addition of $hIAPP_{1-19}$ and $rIAPP_{1-19}$. Figure 4 shows the effect of $hIAPP_{1-19}$, $rIAPP_{1-19}$, and the full-length $rIAPP_{1-37}$ peptide on the intracellular calcium levels of pancreatic islets. Both $hIAPP_{1-19}$ and $rIAPP_{1-19}$ are toxic at relatively low concentrations, as measured by their ability to disrupt the cellular membrane and allow the influx of calcium into the cell. However, $hIAPP_{1-19}$ is significantly more effective than $rIAPP_{1-19}$ at disrupting the islet membrane as shown in Figure 4. The rise in intracellular calcium levels occurred immediately, without the presence of a lag phase that has been detected for the full-length peptide (*15*). Full-length rat IAPP prepared in the same manner does not induce the influx of intracellular calcium into the cell, in agreement with the low cytotoxicity of full-length rIAPP reported in previous studies (*9, 15, 16*).

Comparison of the Binding Affinity of $hIAPP_{1-19}$ and $rIAPP_{1-19}$ for POPG Vesicles. The differences in the membrane disruption induced by $hIAPP_{1-19}$ and $rIAPP_{1-19}$ suggest a difference may exist in the degree of cooperativity in binding to the membrane. Figure 5 shows the binding of $rIAPP_{1-19}$ and $hIAPP_{1-19}$ to POPG vesicles as approximated by the measurement of the conformational changes occurring upon binding to lipid membranes. This method is well established for the qualitative measurement of peptide membrane binding (*44*), although conformational changes occurring after membrane binding can complicate quantitative analysis. Like the full-length peptide, both $hIAPP_{1-19}$ and $rIAPP_{1-19}$ exist in a random coil conformation in solution and adopt an α-helical conformation upon binding to the membrane (*33, 45*). However, noticeable differences can be seen in the binding curves of $hIAPP_{1-19}$ and $rIAPP_{1-19}$ titrated with increasing concentrations of POPG vesicles (Figure 5).

As shown in Figure 5, $rIAPP_{1-19}$ is nearly as effective in binding as $hIAPP_{1-19}$ at saturating concentrations of POPG but is somewhat less effective at lower concentrations. The binding of full-length human and rat IAPP is known to be a cooperative process with membrane binding proceeding much more efficiently after the formation of small aggregates of IAPP on the membrane (*33*). Full-length rat IAPP differs from full-length human IAPP in that the nucleation of small aggregates by rat IAPP is noticeably impaired as compared to that of human IAPP (*33*). The lower affinity of $rIAPP_{1-19}$ for the membrane at lower concentrations of POPG suggests the rat 1−19 fragment, like full-length rIAPP, is impaired in forming the small aggregates that enhance membrane binding.

Interaction of $hIAPP_{1-19}$ and $rIAPP_{1-19}$ with Membrane Determined by Differential Scanning Calorimetry. In the accompanying paper detailing the structures of $hIAPP_{1-19}$ and $rIAPP_{1-19}$ in dodecylphosphocholine (DPC) micelles, we show a significant difference in the accessibility of $hIAPP_{1-19}$ and $rIAPP_{1-19}$ to manganese ions (*39*). This indicates $hIAPP_{1-19}$ is located significantly deeper within the hydrophobic core of the micelle than $rIAPP_{1-19}$ and suggests a different mode for the binding to phospholipid bilayers. To test this model, the interaction of $hIAPP_{1-19}$ and $rIAPP_{1-19}$ peptides with membrane was characterized by differential scanning calorimetry (DSC). In general, the phase behavior of lipid membrane systems is highly affected by the presence of guest molecules such as peptides (*46, 47*). In particular, the effect on the thermally induced gel to liquid-crystalline phase transition and the related thermodynamic variables (melting temperature (T_m), enthalpy change (ΔH), and entropy change (ΔS)) depends on the nature of the interactions between the peptide and the membrane and on the topology of the peptide relative to the lipid bilayer (*48, 49*). A peptide randomly distributed on the surface of the bilayer disorders the surrounding lipids when the membrane is in the gel phase, lowering the ΔH and T_m associated with the gel to liquid-crystalline phase transition. The disruption of the lipid−lipid interactions within the membrane also decreases the stability and rigidity of the membrane and therefore decreases the cooperativity of the phase transition. This results in a decreased sharpness of the peak relative to the pure lipid system. The pretransition, reflective of a change in the orientation of the headgroup of phospholipids, is affected as well. A peptide inserted in a transmembrane orientation has less effect on the physical properties of the membrane because the lipid−lipid interactions are disrupted

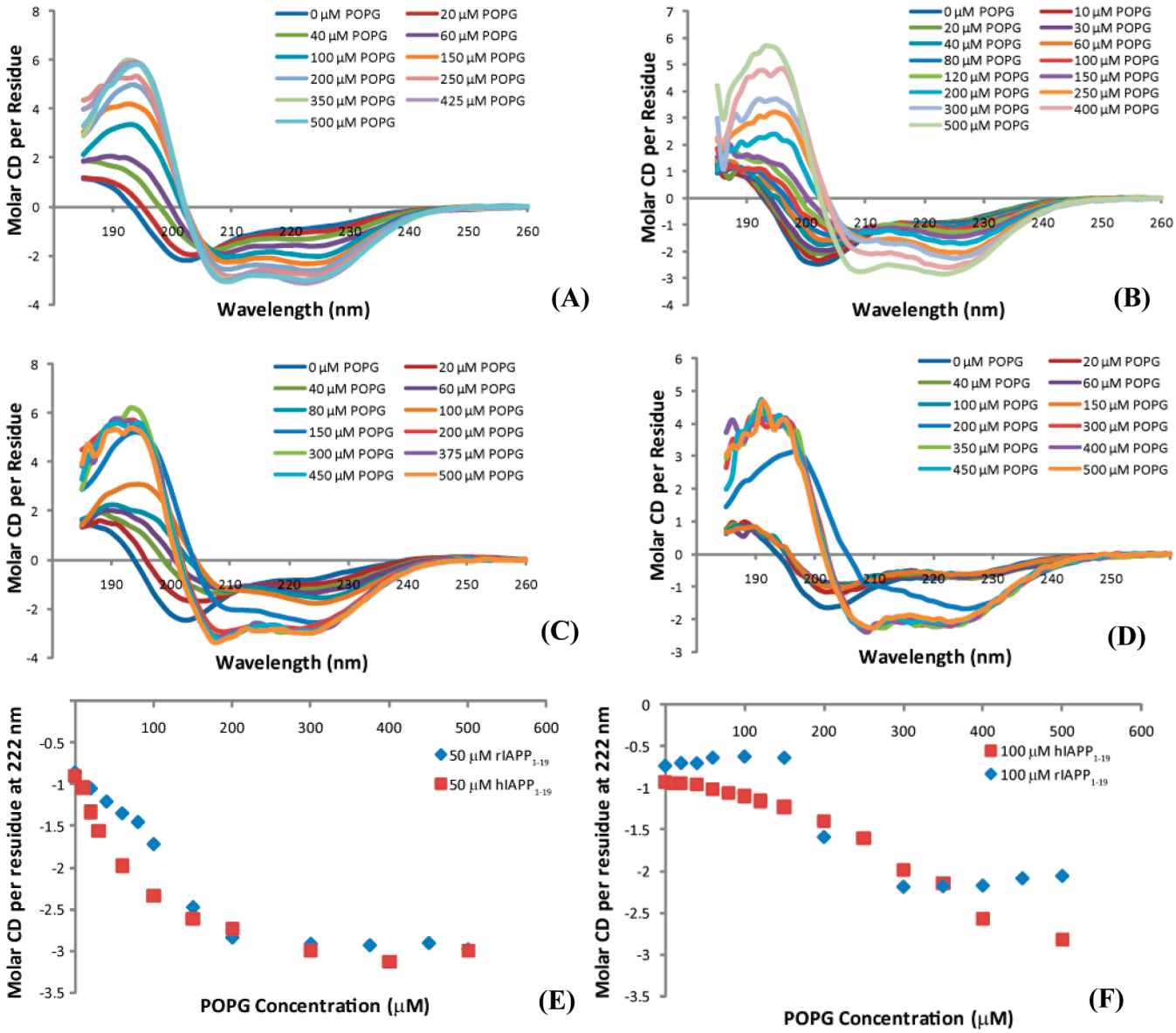

FIGURE 5: CD spectra of 50 μM hIAPP$_{1-19}$ (A), 100 μM hIAPP$_{1-19}$ (B), 50 μM rIAPP$_{1-19}$ (C), and 100 μM rIAPP$_{1-19}$ (D) at the indicated concentrations of POPG. Plots of the molar CD per residue at 222 nm for 50 μM hIAPP$_{1-19}$ and rIAPP$_{1-19}$ (E) and 100 μM hIAPP$_{1-19}$ and rIAPP$_{1-19}$ (F) with the indicated concentrations of POPG. All spectra were obtained in 10 mM sodium phosphate buffer, pH 7.3.

to a much lower degree than with a surface-associated peptide (*49*). The aggregation of the peptide decreases the perturbation on the membrane by decreasing the surface area of the membrane in contact with the peptide (*50, 51*).

Figure 6 shows the effect of hIAPP$_{1-19}$ on mixed DMPC/DMPG vesicles (7/3 ratio). The DSC of pure DMPC/DMPG vesicles shows a single main transition at 24.5 °C indicative of the gel to liquid-crystalline phase transition and a smaller pretransition at 5.4 °C indicative of the rippled gel-to-gel phase transition. The addition of hIAPP$_{1-19}$ up to 2 mol % had a very little effect on the thermodynamics of the gel to liquid-crystalline phase transition. This indicates the lipid−lipid interactions stabilizing the membrane are largely intact and could suggest that the peptide binds in a transmembrane orientation in an aggregated state, as previously inferred for the full-length human peptide (*33, 52, 53*). Self-association of the peptide reduces the number of lipid molecules in contact with the peptide and is therefore expected to decrease the influence of the peptide on the physical properties of the membrane.

Rat IAPP$_{1-19}$ has a much different effect on the membrane (Figure 7). At low concentrations of peptide (0.5−0.75 mol %) the peptide only slightly reduces the ΔH of the main phase transition, but the peptide has a large effect on the pretransition peak reflective of the rippled gel-to-gel phase transition, shifting it to higher temperatures and dramatically increasing the height of the peak for membranes containing 0.5 mol % rIAPP$_{1-19}$. An increase in the pretransition peak height is unusual as most substances tend to reduce the enthalpy change associated with the rippled gel-to-gel phase transition. The rippled gel phase is similar to the gel phase except for the existence of point defects in the bilayer caused by a small percentage of molecules in the fluid phase (*54*). The existence of these defects in turn leads to periodic ripples in the membrane surface. Most peptides disorder the gel phase therefore reducing the enthalpy change associated with the rippled gel-to-gel phase transition as defects are present in both phases. An increase in ΔH for the pretransition can be associated with a decrease in the ripple periodicity, which in turn is related to curvature changes in the membrane

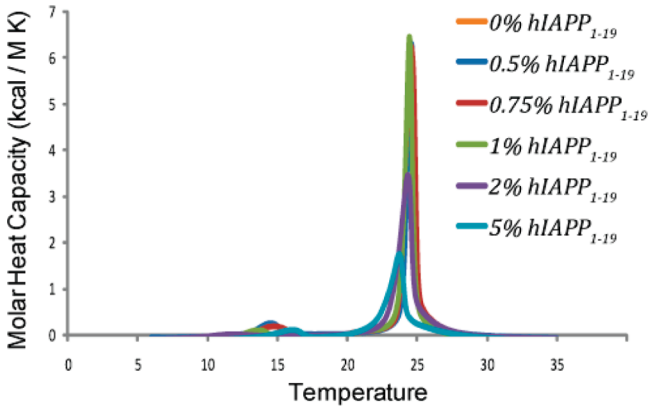

FIGURE 6: Differential scanning calorimetry of the pretransition and the main gel to liquid-crystalline phase transition of DMPC/DMPG (7/3) vesicles at the indicated molar ratio of $hIAPP_{1-19}$ to lipid. Peptide and lipids were codissolved in a chloroform/ethanol solution, dried, and resuspended in sodium phosphate buffer, pH 7.3, with 150 mM NaCl.

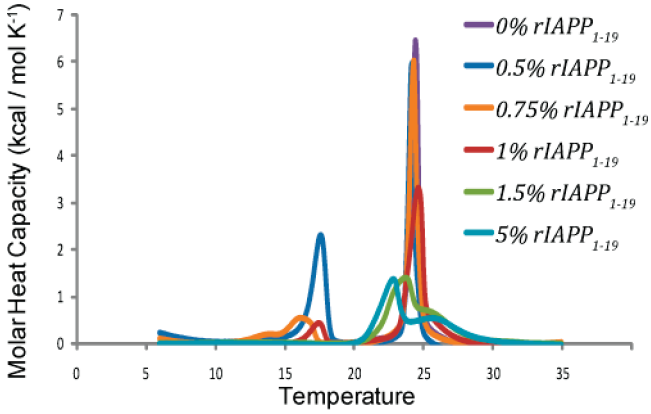

FIGURE 7: Differential scanning calorimetry of the pretransition and the main gel to liquid-crystalline phase transition of DMPC/DMPG (7/3) vesicles at the indicated molar ratio of $rIAPP_{1-19}$ to lipid. Peptide and lipids were codissolved in a chloroform/ethanol solution, dried, and resuspended in 10 mM sodium phosphate buffer, pH 7.3, with 150 mM NaCl.

induced by the mismatch in size between the headgroup region and hydrophobic core of the bilayer induced by the peptide binding to the surface of the membrane (*54, 55*). The formation of ripples in a lipid bilayer has been detected with a surfactant that induces positive curvature in the membrane (*56*). Unlike $hIAPP_{1-19}$, the gel to liquid-crystalline phase transition of membranes containing $rIAPP_{1-19}$ is significantly different at higher concentrations of peptide. At higher concentrations the gel to liquid-crystalline transition is greatly reduced in height and splits into two peaks, one peak with a phase transition at a lower temperature than the pure lipid peak and one peak at a higher temperature than the pure lipid peak. The splitting of a phase transition peak is usually indicative of lipid domain formation, with one peak corresponding to peptide-enriched domains of lipids and the other to peptide-poor domains of lipid (*57, 58*). The greater perturbation of the lipid bilayer by $rIAPP_{1-19}$ indicated by the DSC results suggests that, unlike $hIAPP_{1-19}$, $rIAPP_{1-19}$ may be bound to the surface of the bilayers and not in the active conformation necessary to form pores. This is consistent with the membrane orientation of IAPP peptides determined from our NMR studies (*39*).

CONCLUSIONS

The 1−19 peptide fragment of human IAPP (or amylin) is of particular interest in amyloidogenic protein research as it disrupts model anionic membranes to a near-identical extent as the full-length IAPP peptide but is conformationally stable; once bound to the membrane in an active α-helical form, it does not proceed to form amyloid fibers (*25*). This feature is important for the study of the IAPP peptide, whose rapid and complex aggregation process leads to considerable difficulties in biophysical studies. One of the key arguments for the importance of IAPP amyloid fibers, rather than other oligomeric states of the peptide, in the death of β-cells during type II diabetes is the lack of toxicity of the nonamyloidogenic rat version of the peptide. In light of the nearly identical sequences of the rat and human versions of IAPP sequence in the 1−19 region of the peptide, the membrane disrupting effect of $hIAPP_{1-19}$ is surprising. In this study, we confirmed that the membrane-disrupting activity previously reported for highly charged model membranes also exists for islet cells under physiological conditions. Our results suggest an important role for His18 in the early stages of aggregation and membrane binding. Histidine-18 has previously been implicated in the rate of assembly of amyloid fibers, with amyloid fiber formation proceeding much more slowly when His18 is protonated at a low pH (*38*). In fact, the R18H substitution in the $rIAPP_{1-37}$ is sufficient to turn the peptide from being nonamyloidogenic to slightly amyloidogenic, which is most likely due to the disruption of the stacking of the β-sheets forming the amyloid fiber by the protonated arginine residue (*59*). However, mature amyloid fibers show relatively little toxicity to β-cells, and a different mechanism is likely to operate during the earlier stages of aggregation where the toxicity of the peptide is highest and large aggregates are absent. Our results show, for the relatively nonamyloidogenic but toxic 1−19 fragments of the peptide, that the His18 residue also plays a key role in controlling the toxicity of the peptide by modulating the interactions of IAPP with the phospholipid membrane.

ACKNOWLEDGMENT

The authors thank Professor Ari Gafni and his research group for their interest in this work and for generous access to their CD spectrometer.

REFERENCES

1. Clark, A., and Nilsson, M. R. (2004) Islet amyloid: a complication of islet dysfunction or an aetiological factor in type 2 diabetes? *Diabetologia 47*, 157–169.
2. Hoppener, J. W. M., and Lips, C. J. M. (2006) Role of islet amyloid in type 2 diabetes mellitus. *Int. J. Biochem. Cell Biol. 38*, 726–736.
3. Lorenzo, A., and Yankner, B. A. (1996) Amyloid fibril toxicity in Alzheimer's disease and diabetes, in *Neurobiology of Alzheimer's Disease*, pp 89−95.
4. Matveyenko, A. V., and Butler, P. C. (2006) Islet amyloid polypeptide (IAPP) transgenic rodents as models for type 2 diabetes. *ILAR J. 47*, 225–233.
5. Haataja, L., Gurlo, T., Huang, C. J., and Butler, P. C. (2008) Islet amyloid in type 2 diabetes, and the toxic oligomer hypothesis. *Endocr. Rev. 29*, 302–316.
6. Hoppener, J. W. M., Oosterwijk, C., Nieuwenhuis, M. G., Posthuma, G., Thijssen, J. H. H., Vroom, T. M., Ahren, B., and Lips, C. J. M. (1999) Extensive islet amyloid formation is induced by development of type II diabetes mellitus and contributes to its

progression: pathogenesis of diabetes in a mouse model. *Diabetologia 42*, 427–434.
7. Soeller, W. C., Janson, J., Hart, S. E., Parker, J. C., Carty, M. D., Stevenson, R. W., Kreutter, D. K., and Butler, P. C. (1998) Islet amyloid-associated diabetes in obese A(vy)/a mice expressing human islet amyloid polypeptide. *Diabetes 47*, 743–750.
8. Matveyenko, A. V., and Butler, P. C. (2006) Beta-cell deficit due to increased apoptosis in the human islet amyloid polypeptide transgenic (HIP) rat recapitulates the metabolic defects present in type 2 diabetes. *Diabetes 55*, 2106–2114.
9. Huang, C. J., Haataja, L., Gurlo, T., Butler, A. E., Wu, X., Soeller, W. C., and Butler, P. C. (2007) Induction of endoplasmic reticulum stress-induced beta-cell apoptosis and accumulation of polyubiquitinated proteins by human islet amyloid polypeptide. *Am. J. Physiol. Endocrinol. Metab. 293*, E1656–E1662.
10. Janson, J., Soeller, W. C., Roche, P. C., Nelson, R. T., Torchia, A. J., Kreutter, D. K., and Butler, P. C. (1996) Spontaneous diabetes mellitus in transgenic mice expressing human islet amyloid polypeptide. *Proc. Natl. Acad. Sci. U.S.A. 93*, 7283–7288.
11. Butler, A. E., Janson, J., Soeller, W. C., and Butler, P. C. (2003) Increased beta-cell apoptosis prevents adaptive increase in beta-cell mass in mouse model of type 2 diabetes—Evidence for role of islet amyloid formation rather than direct action of amyloid. *Diabetes 52*, 2304–2314.
12. Hull, R. L., Shen, Z. P., Watts, M. R., Kodama, K., Carr, D. B., Utzschneider, K. M., Zraika, S., Wang, F., and Kahn, S. E. (2005) Long-term treatment with rosiglitazone and metformin reduces the extent of, but does not prevent, islet antyloid deposition in mice expressing the gene for human islet antyloid polypeptide. *Diabetes 54*, 2235–2244.
13. Tasaka, Y., Nakaya, F., Matsumoto, H., Iwamoto, Y., and Omori, Y. (1995) Pancreatic amylin content in human diabetic subjects and its relation to diabetes. *Pancreas 11*, 303–308.
14. Bell, E. T. (1959) Hyalinization of the islets of Langerhans in nondiabetic individuals. *Am. J. Pathol. 35*, 801–805.
15. Demuro, A., Mina, E., Kayed, R., Milton, S. C., Parker, I., and Glabe, C. G. (2005) Calcium dysregulation and membrane disruption as a ubiquitous neurotoxic mechanism of soluble amyloid oligomers. *J. Biol. Chem. 280*, 17294–17300.
16. Janson, J., Ashley, R. H., Harrison, D., McIntyre, S., and Butler, P. C. (1999) The mechanism of islet amyloid polypeptide toxicity is membrane disruption by intermediate-sized toxic amyloid particles. *Diabetes 48*, 491–498.
17. Konarkowska, B., Aitken, J. F., Kistler, J., Zhang, S. P., and Cooper, G. J. S. (2006) The aggregation potential of human amylin determines its cytotoxicity towards islet beta-cells. *FEBS J. 273*, 3614–3624.
18. Meier, J. J., Kayed, R., Lin, C. Y., Gurlo, T., Haataja, L., Jayasinghe, S., Langen, R., Glabe, C. G., and Butler, P. C. (2006) Inhibition of human IAPP fibril formation does not prevent beta-cell death: evidence for distinct actions of oligomers and fibrils of human IAPP. *Am. J. Physiol. 291*, E1317—E1324.
19. Ritzel, R. A., and Butler, P. C. (2003) Replication increases beta-cell vulnerability to human islet amyloid polypeptide-induced apoptosis. *Diabetes 52*, 1701–1708.
20. Anguiano, M., Nowak, R. J., and Lansbury, P. T. (2002) Protofibrillar islet amyloid polypeptide permeabilizes synthetic vesicles by a pore-like mechanism that may be relevant to type II diabetes. *Biochemistry 41*, 11338–11343.
21. Lin, C. Y., Gurlo, T., Kayed, R., Butler, A. E., Haataja, L., Glabe, C. G., and Butler, P. C. (2007) Toxic human islet amyloid polypeptide (h-IAPP) oligomers are intracellular, and vaccination to induce anti-toxic oligomer antibodies does not prevent h-IAPP-induced beta-cell apoptosis in h-IAPP transgenic mice. *Diabetes 56*, 1324–1332.
22. Quist, A., Doudevski, L., Lin, H., Azimova, R., Ng, D., Frangione, B., Kagan, B., Ghiso, J., and Lal, R. (2005) Amyloid ion channels: A common structural link for protein-misfolding disease. *Proc. Natl. Acad. Sci. U.S.A. 102*, 10427–10432.
23. (a) Porat, Y., Kolusheva, S., Jelinek, R., and Gazit, E. (2003) The human islet amyloid polypeptide forms transient membrane-active prefibrillar assemblies. *Biochemistry 42*, 10971–10977. (b) Brender, J. R., Dürr, U. H. N., Heyl, D., Budarapu, M. B., and Ramamoorthy, A. (2007) Membrane fragmentation by human islet amyloid polypeptide detected by solid-state NMR spectroscopy of membrane nanotubes. *Biochim. Biophys. Acta 1768*, 2026–2029.
24. Powers, E. T., and Powers, D. L. (2008) Mechanisms of protein fibril formation: Nucleated polymerization with competing off-pathway aggregation. *Biophys. J. 94*, 379–391.
25. Brender, J. R., Lee, E. L., Cavitt, M. A., Gafni, A., Steel, D. G., and Ramamoorthy, A. (2008) Amyloid fiber formation and membrane disruption are separate processes localized in two distinct regions of IAPP, the type-2-diabetes-related peptide. *J. Am. Chem. Soc. 130*, 6424–6429.
26. Khemtemourian, L., Killian, J. A., Hoppener, J. W., and Engel, M. F. (2008) (2008) Recent insights in islet amyloid polypeptide-induced membrane disruption and its role in beta-cell death in type 2 diabetes mellitus. *Exp. Diabetes Res.* 421287.
27. Necula, M., Kayed, R., Milton, S., and Glabe, C. G. (2007) Small molecule inhibitors of aggregation indicate that amyloid beta oligomerization and fibrillization pathways are independent and distinct. *J. Biol. Chem. 282*, 10311–10324.
28. Yoshiike, Y., Kayed, R., Milton, S. C., Takashima, A., and Glabe, C. G. (2007) Pore-forming proteins share structural and functional homology with amyloid oligomers. *Neuromol. Med. 9*, 270—275.
29. Pralong, W. F., Bartley, C., and Wollheim, C. B. (1990) Single islet beta-cell stimulation by nutrients—Relationship between pyridine-nucleotides, cytosolic Ca^{2+} and secretion. *EMBO J. 9*, 53–60.
30. Bechinger, B., and Lohner, K. (2006) Detergent-like actions of linear amphipathic cationic antimicrobial peptides. *Biochim. Biophys. Acta 1758*, 1529–1539.
31. Shai, Y. (1999) Mechanism of the binding, insertion and destabilization of phospholipid bilayer membranes by α-helical antimicrobial and cell non-selective membrane-lytic peptides. *Biochim. Biophys. Acta 1462*, 55–70.
32. Hoskin, D. W., and Ramamoorthy, A. (2008) Studies on anticancer activities of antimicrobial peptides. *Biochim. Biophys. Acta 1778*, 357–375.
33. Knight, J. D., Hebda, J. A., and Miranker, A. D. (2006) Conserved and cooperative assembly of membrane-bound α-helical states of islet amyloid polypeptide. *Biochemistry 45*, 9496–9508.
34. Vanhulst, K. L., Hackeng, W. H. L., Hoppener, J. W. M., Vanjaarsveld, B. C., Nieuwenhuis, M. G., Blankenstein, M. A., and Lips, C. J. M. (1994) An improved method for the determination of islet amyloid polypeptide levels in plasma. *Ann. Clin. Biochem. 31*, 165–170.
35. Ariga, T., McDonald, M. P., and Yu, R. K. (2008) Role of ganglioside metabolism in the pathogenesis of Alzheimer's disease—a review. *J. Lipid Res. 49*, 1157–1175.
36. Lee, S. J., Liyanage, U., Bickel, P. E., Xia, W. M., Lansbury, P. T., and Kosik, K. S. (1998) A detergent-insoluble membrane compartment contains A beta in vivo. *Nat. Med. 4*, 730–734.
37. Jaikaran, E., Higham, C. E., Serpell, L. C., Zurdo, J., Gross, M., Clark, A., and Fraser, P. E. (2001) Identification of a novel human islet amyloid polypeptide beta-sheet domain and factors influencing fibrillogenesis. *J. Mol. Biol. 308*, 515–525.
38. Abedini, A., and Raleigh, D. P. (2005) The role of His-18 in amyloid formation by human islet amyloid polypeptide. *Biochemistry 44*, 16284–16291.
39. Nanga, R. P. R., Brender, J. R., Xu, J., Veglia, G., and Ramamoorthy, A. (2008) Structures of rat and human islet amyloid polypeptide $IAPP_{1-19}$ in micelles by NMR spectroscopy. *Biochemistry 47*, 12689–12697.
40. Kawahara, M., Kuroda, Y., Arispe, N., and Rojas, E. (2000) Alzheimer's beta-amyloid, human islet amylin, and prion protein fragment evoke intracellular free calcium elevations by a common mechanism in a hypothalamic GnRH neuronal cell line. *J. Biol. Chem. 275*, 14077–14083.
41. Mattson, M. P., and Goodman, Y. (1995) Different amyloidogenic peptides share a similar mechanism of neurotoxicity involving reactive oxygen species and calcium. *Brain Res. 676*, 219—224.
42. Casas, S., Gomis, R., Gribble, F. M., Altirriba, J., Knuutila, S., and Novials, A. (2007) Impairment of the ubiquitin-proteasome pathway is a downstream endoplasmic reticulum stress response induced by extracellular human islet amyloid polypeptide and contributes to pancreatic beta-cell apoptosis. *Diabetes 56*, 2284–2294.
43. Casas, S., Novials, A., Reimann, F., Gomis, R., and Gribble, F. M. (2008) Calcium elevation in mouse pancreatic beta cells evoked by extracellular human islet amyloid polypeptide involves activation of the mechanosensitive ion channel TRPV4. *Diabetologia* (in press).
44. Ladokhin, A. S., and White, S. H. (1999) Folding of amphipathic alpha-helices on membranes: Energetics of helix formation by melittin. *J. Mol. Biol. 285*, 1363–1369.

45. Jayasinghe, S. A., and Langen, R. (2005) Lipid membranes modulate the structure of islet amyloid polypeptide. *Biochemistry 44*, 12113–12119.
46. Pappalardo, G., Milardi, D., Magri, A., Attanasio, F., Impellizzeri, G., La Rosa, C., Grasso, D., and Rizzarelli, E. (2007) Environmental factors differently affect human and rat IAPP: Conformational preferences and membrane interactions of IAPP17−29 peptide derivatives. *Chem.-Eur. J. 13*, 10204–10215.
47. Grasso, D., Milardi, D., La Rosa, C., and Rizzarelli, E. (2001) DSC study of the interaction of the prion peptide PrP106−126 with artificial membranes. *New J. Chem. 25*, 1543–1548.
48. Henzler-Wildman, K. A., Martinez, G. V., Brown, M. F., and Ramamoorthy, A. (2004) Perturbation of the hydrophobic core of lipid bilayers by the human antimicrobial peptide LL-37. *Biochemistry 43*, 8459–8469.
49. McElhaney, R. N. (1986) Differential scanning calorimetric studies of lipid protein interactions in model membrane systems. *Biochim. Biophys. Acta 864*, 361–421.
50. Ivanova, V. P., Makarov, I. M., Schaffer, T. E., and Heimburg, T. (2003) Analyzing heat capacity profiles of peptide-containing membranes: cluster formation of gramicidin A. *Biophys. J. 84*, 2427–2439.
51. Ramamoorthy, A., Lee, D. K., Santos, J. S., and Henzler-Wildman, K. A. (2008) Nitrogen-14 solid-state NMR spectroscopy of aligned phospholipid bilayers to probe peptide-lipid interaction and oligomerization of membrane associated peptides. *J. Am. Chem. Soc. 130*, 11023–11029.
52. Knight, J. D., and Miranker, A. D. (2004) Phospholipid catalysis of diabetic amyloid assembly. *J. Mol. Biol. 341*, 1175–1187.
53. Mishra, R., Bulic, B., Sellin, D., Jha, S., Waldmann, H., and Winter, R. (2008) Small-molecule inhibitors of islet amyloid polypeptide fibril formation. *Angew. Chem., Int. Ed. Engl. 47*, 4679–4682.
54. Heimburg, T. (2000) A model for the lipid pretransition: Coupling of ripple formation with the chain-melting transition. *Biophys. J. 78*, 1154–1165.
55. Sun, X. Q., and Gezelter, J. D. (2008) Dipolar ordering in the ripple phases of molecular-scale models of lipid membranes. *J. Phys. Chem. B 112*, 1968–1975.
56. Brasseur, R., Braun, N., El Kirat, K., Deleu, M., Mingeot-Leclercq, M. P., and Dufrene, Y. F. (2007) The biologically important surfactin lipopeptide induces nanoripples in supported lipid Bilayers. *Langmuir 23*, 9769–9772.
57. Epand, R. M. (2007) Detecting the presence of membrane domains using DSC. *Biophys. Chem. 126*, 197–200.
58. Epand, R. F., Schmitt, M. A., Gellman, S. H., and Epand, R. M. (2006) Role of membrane lipids in the mechanism of bacterial species selective toxicity by two alpha/beta-antimicrobial peptides. *Biochim. Biophys. Acta 1758*, 1343–1350.
59. Green, J., Goldsbury, C., Min, T., Sunderji, S., Frey, P., Kistler, J., Cooper, G., and Aebi, U. (2003) Full-length rat amylin forms fibrils following substitution of single residues from human amylin. *J. Mol. Biol. 326*, 1147–1156.

BI801427C